Complete and incomplete fusion in $^{20}Ne + ^{93}Nb$ reactions

D. J. Parker
Nuclear Physics Division, Harwell Laboratory, Oxfordshire, OX11 0RA, United Kingdom

J. J. Hogan
Department of Chemistry, McGill University, Montreal, Quebec, Canada H3A 2K6

J. Asher
Nuclear Physics Division, Harwell Laboratory, Oxfordshire, OX11 0RA, United Kingdom
(Received 18 August 1986)

Cross sections for production of radioactive product residues from reactions of ^{20}Ne on ^{93}Nb have been measured at incident energies of 106 and 148 MeV. Detailed differential recoil range distributions have been measured for many of these products, and show evidence of several incomplete fusion processes in addition to complete fusion. The inclusive spectra of emitted protons, alpha particles, and projectilelike fragments have been measured at the same incident energies, and show components consistent with some form of projectile breakup. These breakup fragments are hypothesized to be the spectator fragments arising from incomplete fusion. Whereas the recoil range distribution data cannot be accounted for by statistical model calculations assuming only complete fusion, inclusion of the various incomplete fusion processes on the basis of the above hypothesis does reproduce the data. There is also an indication of direct transfer processes contributing to formation of near-target products.

I. INTRODUCTION

It is now generally recognized that several different reaction mechanisms are important in reactions of light heavy ions, even at incident energies as low as 5 MeV per nucleon. These processes may be broadly classified in terms of the degree of momentum transfer from the projectile to the targetlike product(s) in the first stage of the reaction. Three important classes of process are as follows: (i) complete fusion, involving full momentum transfer; (ii) incomplete fusion, in which some part of the projectile behaves essentially as a spectator while the remainder fuses with the target, leading to transfer of a fraction of the incident momentum essentially equal to the fraction of the projectile mass that fuses; and (iii) direct reactions, involving transfer of a single nucleon or cluster in a grazing collision, with very little momentum transfer. At higher incident energies (above about 10 MeV per nucleon) preequilibrium emission processes also become important.

For a particular reaction, measurement of the recoil velocity of the heavy product, or, equivalently, its recoil range in some stopping medium, can be used to determine the momentum transfer. Where the product is a radionuclide, the distribution of recoil ranges associated with its formation can be simply determined by using a catcher of suitable geometry, counted off-line. Such recoil studies recently proved particularly successful[1] in establishing the importance of two distinct incomplete fusion processes in reactions of ^{12}C with ^{51}V, and in determining the cross section for each process as a function of projectile energy up to 100 MeV. Reactions induced by ^{20}Ne are expected to be considerably more complex than those of ^{12}C, and it is of interest to see whether the same experimental techniques yield similarly useful information for ^{20}Ne-induced reactions.

The distinction between processes (ii) and (iii) has long been accepted in principle, but has not always been clear for individual reactions. As long ago as 1961, Kaufman and Wolfgang[2] showed the existence of rather inelastic grazing processes in multinucleon transfer reactions of ^{12}C, ^{14}N, and ^{16}O, in contrast to the direct "tunneling" process which dominates single nucleon transfer. Subsequent work,[3] generally using recoil techniques, confirmed that processes intermediate between complete fusion and direct transfer are important in forming products somewhat heavier than the target.

However, a consistent appreciation of the process now referred to as incomplete fusion only really emerged with the work of Inamura *et al.*[4] from 1977 onwards, using particle/γ coincidence measurements of the projectilelike fragment.[5] This technique is most useful for systems sufficiently heavy that evaporation of charged particles from the excited compound system is effectively inhibited by the Coulomb barrier. Careful recoil studies, on the other hand, may be more powerful in distinguishing different incomplete fusion processes in lighter systems where the same product may be formed by more than one fusion process, followed by different degrees of charged particle evaporation. The mass regime involved in reactions of ^{20}Ne on ^{93}Nb, although quite different from that investigated in our previous $^{12}C + ^{51}V$ study, is nevertheless still within the region in which charged particle evaporation is important.

We recently reported[6] recoil studies of radioactive products from reactions of ^{20}Ne on ^{93}Nb at approximately 100

and 142 MeV. By means of thick-target/thick-catcher measurements, it was possible to determine the mean recoil range of each product parallel to, and in some cases also perpendicular to, the beam axis. The mean recoil range was found to decrease monotonically with decreasing product mass, from a value corresponding to essentially 100% momentum transfer for the heaviest detected products (complete fusion) down to a value corresponding to less than 20% momentum transfer for near target products. These data indicated that several different incomplete fusion processes, as well as complete fusion, compete in these reactions and contribute in differing degrees to formation of individual products; however, it is not possible to isolate these processes from such an integral study.

For a number of these products, in addition to determining production cross sections, we have now measured full differential recoil range distributions at 106 and 148 MeV, with the aim of distinguishing contributions from different processes. Although the separate contributions to formation of a particular product are not fully resolved and cannot in general be unambiguously identified in the measured distributions, these show clear evidence that several different incomplete fusion processes are present. At the lower of the two energies studied, some products

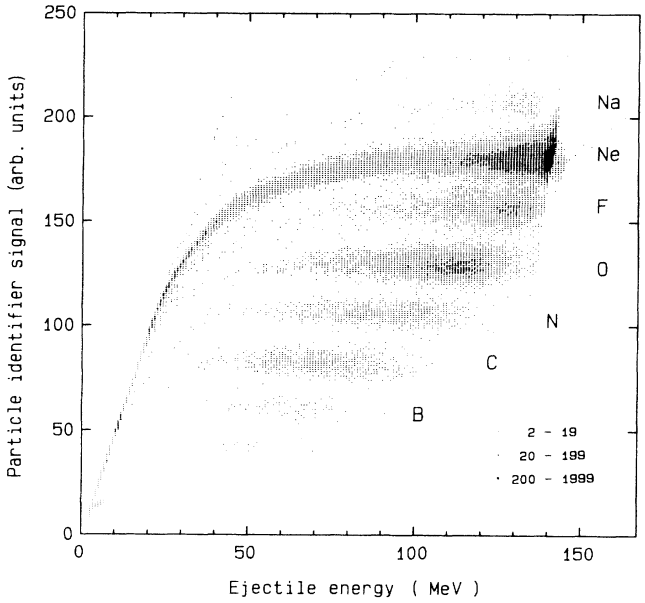

FIG. 1. Map of particle identifier function versus particle energy obtained from reactions of 148 MeV ^{20}Ne with ^{93}Nb at a laboratory angle of 30°.

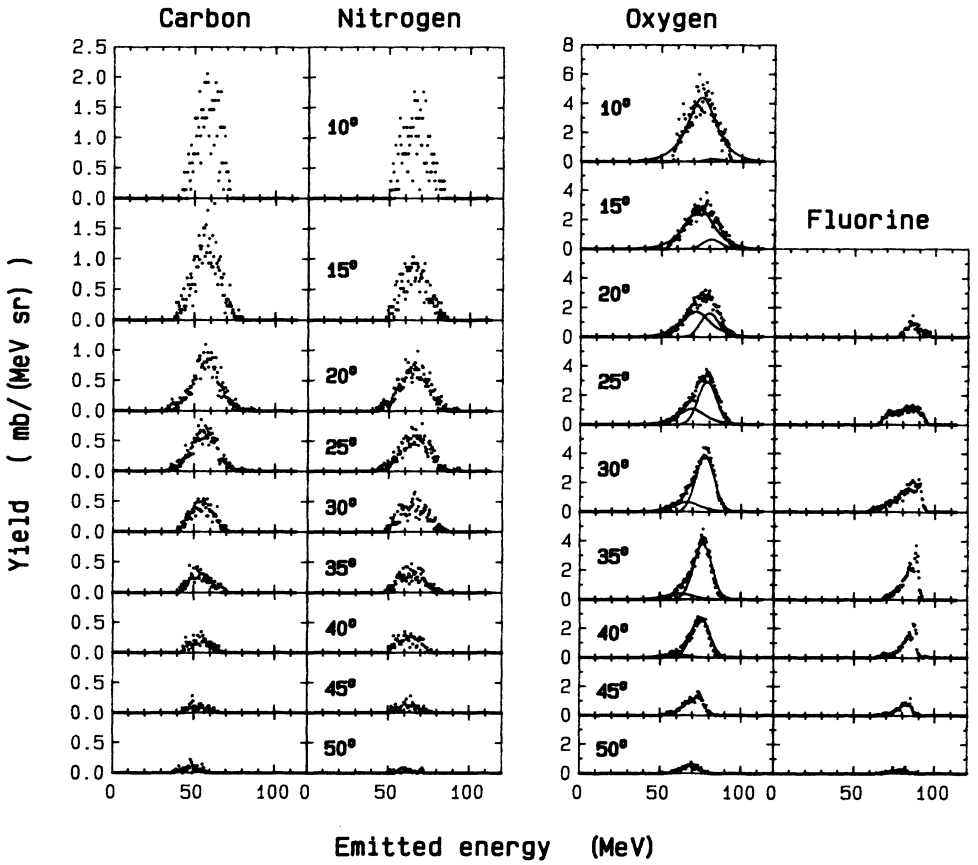

FIG. 2. Projectilelike fragment spectra measured at 106 MeV. The smooth curves in the oxygen spectra show the decomposition of these spectra into two components, as described in the text.

are apparently formed predominantly by a single incomplete fusion process.

To complement these recoil studies of the heavy products, we have measured the inclusive energy spectra of light charged particles emitted at a number of laboratory angles. These show components attributable to breakup of the ^{20}Ne projectile, producing a variety of fragments from alpha particles to fluorine; we have established the total yield of each type of fragment.

These projectilelike fragments, emitted with near beam velocity, must include the "spectator" fragments from any incomplete fusion processes which are present. We have attempted to account for our measured yields of heavy residues, and for the shapes of the measured recoil distributions, on the hypothesis that essentially all of the observed projectilelike fragments are associated with incomplete fusion. Modeling, based on the measured spectra of projectilelike fragments, and making use of the statistical model code CASCADE (Ref. 7) to predict the population of final residues following particle evaporation, is able to account rather well for all the recoil distributions and absolute production cross sections measured for products heavier than mass 96.

The spectra of emitted oxygen and fluorine also contain components characteristic of direct transfer rather than incomplete fusion. It appears to be impossible to explain the yields of near-target products on the basis of incomplete fusion processes alone; presumably various direct transfer processes are important here, but this study was unable to identify these in detail.

Section II of this paper describes the experimental techniques used in this work, and Sec. III provides a brief qualitative overview of the data obtained. In Sec. IV the modeling used to calculate the yields of individual final products arising from complete and incomplete fusion, from the measured projectilelike fragment spectra, is developed, and in Sec. V the results of these calculations are compared to the data.

II. EXPERIMENTAL METHOD

A. Particle spectra

The energy spectra of protons, alpha particles, boron, carbon, nitrogen, oxygen, and fluorine emitted during the reactions of 106 and 148 MeV ^{20}Ne with ^{93}Nb were measured at a number of laboratory angles between 10° and 150°, using a $\Delta E/E$ telescope of silicon surface barrier detectors.

Beams of 106 MeV $^{20}Ne^{5+}$ and 148 MeV $^{20}Ne^{6+}$ from the Harwell Variable Energy Cyclotron (VEC) were used; the beam collimation and detector geometry were as reported previously.[1] The targets used were rolled foils of niobium, between 0.7 and 1.2 mg/cm^2 thick, mounted normal to the beam axis except during measurements made at angles close to 90° when the target angle was displaced by 15° so as to avoid masking the detectors. The

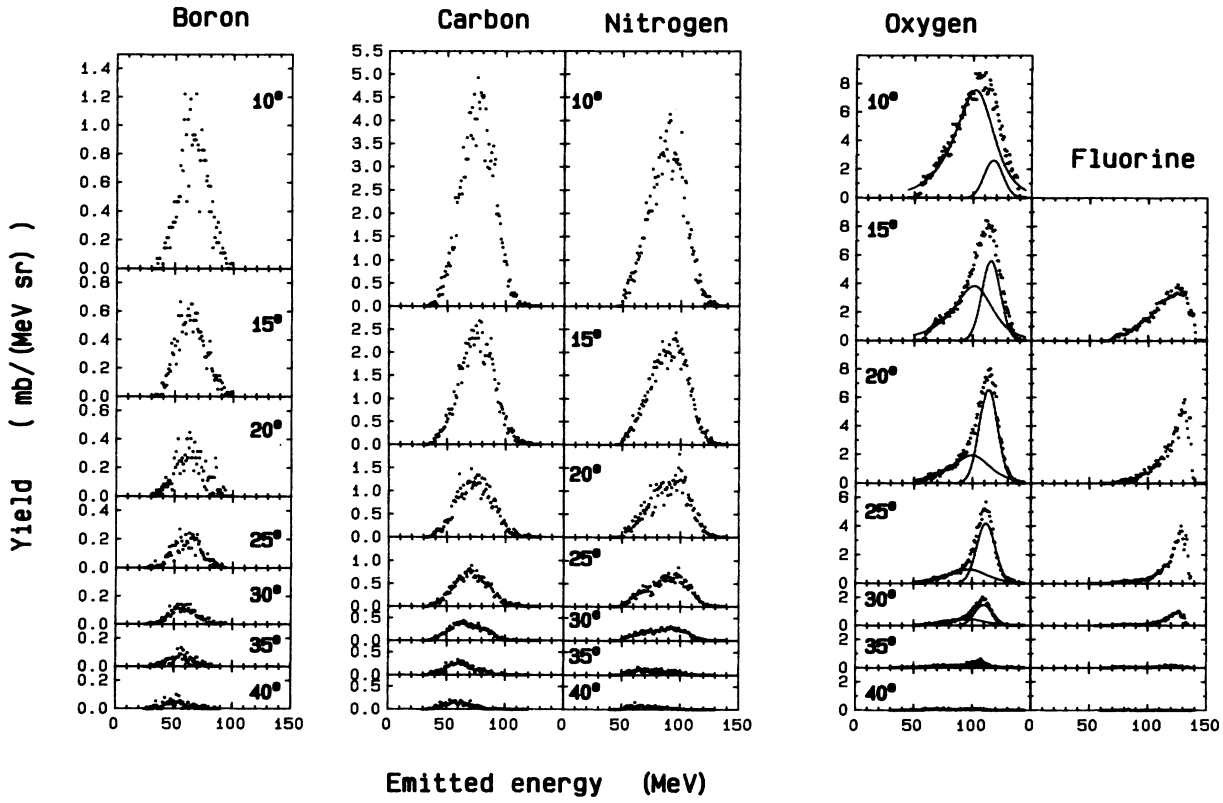

FIG. 3. As Fig. 2, at 148 MeV.

targets were nominally 99.99% pure; light impurities (principally hydrogen and oxygen) were found by elastic recoil detection analysis to be present at levels below 5 at. %.

The signals from the E and ΔE detectors were fed to two analog to digital converters (ADC's), whose inputs were gated so as to receive only events having a valid pair of ΔE and E signals; the data were stored event-by-event using a PDP 11/34 computer. Subsequently the data were sorted into two-parameter maps of total energy, $E+\Delta E$, versus a characteristic particle identifier constructed as

$$[(E+\Delta E)^{1.67}-E^{1.67}]^{0.67} .$$

The energy calibration of the two signals was established from the pulse height generated in each of the two detectors by the elastically-scattered ^{20}Ne detected at forward angles, using the range/energy relation of Littmark and Ziegler[8] for ^{20}Ne in silicon to determine the respective energies expected in the two detectors. In the resulting maps, an example of which is shown in Fig. 1, clearly resolved ridges corresponding to various different elements were observed; the energy spectrum for a given Z was then obtained by projecting out from the map the relevant ridge. For elements above $Z=4$, it was not in general possible to resolve contributions from different isotopes of the same element.

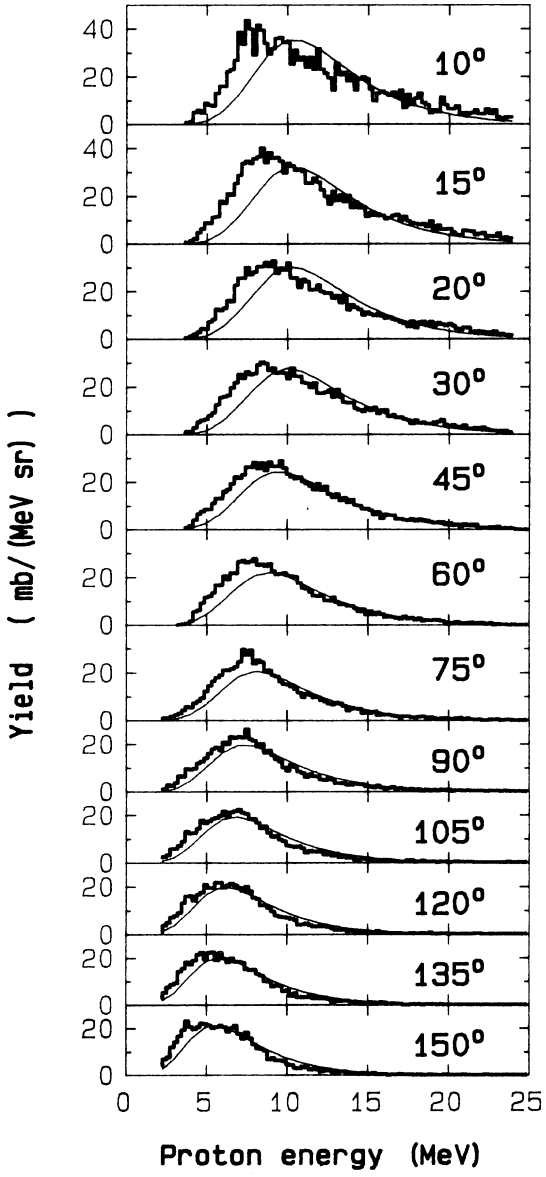

FIG. 4. Proton spectra measured at 148 MeV (histograms). The smooth curves show the evaporation spectra calculated by CASCADE, fitted to the data.

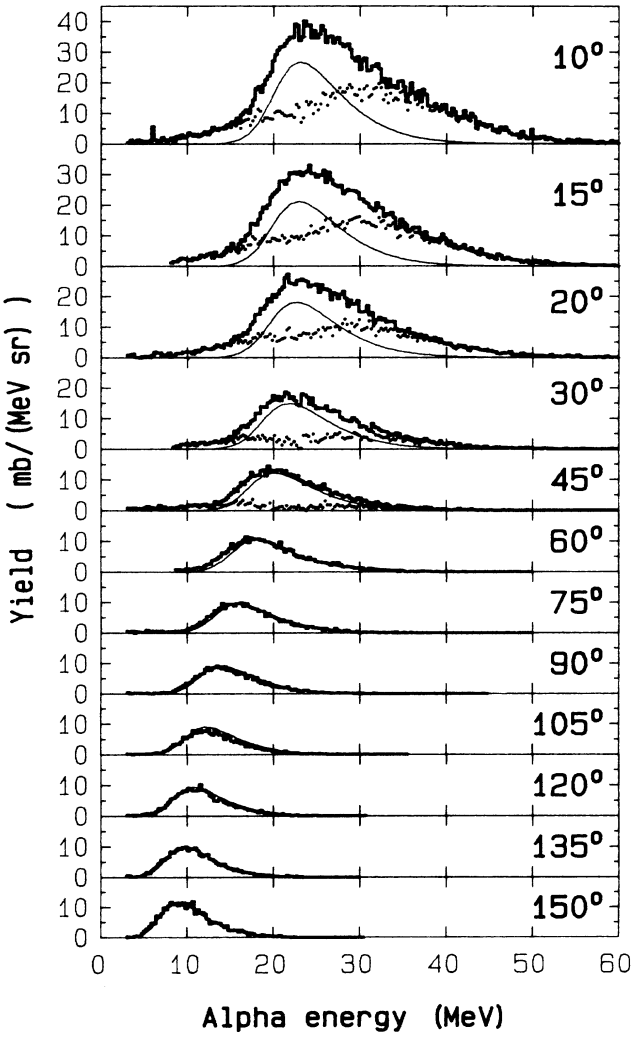

FIG. 5. Alpha particle spectra measured at 148 MeV (histograms). The smooth curves show the evaporation spectra calculated by CASCADE, fitted to the data at backward angles; the points show the result of subtracting these curves from the data at forward angles.

The E detector used was 3 mm thick. A 10 or 15 μm thick ΔE detector was used to detect alpha particles with energies below 20 MeV, and all the heavier species; a 50 μm detector was used to measure the alpha particle spectra above 10 MeV, and the proton spectra. In the region of overlap between 10 and 20 MeV, the alpha spectra measured using the different ΔE detectors agreed very well.

In a few of the forward angle runs, a more complicated telescope was used, consisting of two ΔE detectors (15 μm and 10 μm, respectively) followed by the E detector; the second ΔE detector assisted in discriminating against the elastically-scattered beam, which limited the usable beam current at the most forward angles.

The transmitted beam was collected in an electrically-suppressed Faraday cup. The measured spectra have been normalized so as to give the double-differential cross section, $d^2\sigma/dE\,d\Omega$, in mb/(MeV sr), using the measured beam fluence, the known detector solid angle (0.38 msr), and the estimated target thickness. The principal contribution to uncertainty in absolute normalization arose from a 15% uncertainty in target thickness. The relative normalization of the various spectra should, however, be consistent to better than 5%.

The spectra of ions with $5 \leq Z \leq 9$ observed at 106 and at 148 MeV are shown in Figs. 2 and 3, respectively; the proton and alpha particle spectra observed at 148 MeV are shown in Figs. 4 and 5, respectively (the spectra at 106 MeV are quite similar). No significant yields of lithium or beryllium, or of the other isotopes of hydrogen or helium, were observed in this work.

B. Product cross sections

The absolute cross sections for producing approximately 25 distinct radioactive reaction residues from reactions of ^{20}Ne on ^{93}Nb were measured at incident energies of 106 and 148 MeV by irradiating a thin niobium target, backed by a thick aluminum catcher, and using off-line gamma-ray spectrometry to determine the yields of product residues.

A single irradiation was performed at each of the two energies. For each, the target used consisted of 250 $\mu g/cm^2$ Nb deposited by sputtering onto a backing of 200 $\mu g/cm^2$ Al; a 15 μm Al catcher was placed behind the target to catch recoiling products. The thickness of the Nb layer had been determined prior to irradiation, to an uncertainty of less than 10%, by a Rutherford backscattering technique. For each irradiation the VEC beam was collimated to a spot diameter of 5 mm; the target and the catcher were mounted inside an electrically-suppressed Faraday cup and irradiated to a total fluence of 100 particle μC at a current of approximately 10 particle nA; a record was maintained of total fluence versus time.

Following irradiation, the target and catcher were counted together at a distance of 75 mm from a 25%-efficient Ge(Li) detector. A continuous sequence of counts was performed, starting 20 min after the end of irradiation and continuing for 15 d.

The computer code GAMANAL (Ref. 9) was used to find and integrate the peaks in the γ-ray spectra; the resulting intensities were normalized to take account of the efficiency of the detector, which had been measured (to an uncertainty of 5%) as a function of γ-ray energy in this geometry. Decay curve analysis was performed to extract the initial activity value for each detected radionuclide, and this was converted to a production cross section using the known target thickness and beam fluence. Data on γ-ray energies, branching ratios, and half-lives were extracted from the GSI Gamma Catalog.[10] Correction was made for the effect for decay during irradiation, taking account of the recorded variation of beam current versus time.

The normalization of the cross sections obtained is believed to be accurate to better than 15%. The statistical uncertainty in determining individual product yields was generally less than 10%, but in a few cases the counting statistics were poorer.

Table I lists the nuclides for which results were obtained, together with the γ-ray lines and half-lives used. Two points should be noted. Firstly, there is extensive feeding of many of the observed radionuclides by beta-decay precursors. Meaningful results can be obtained only if the primordial yield of a given nuclide can be extracted (by decay curve analysis) or if the half-lives of the precursors are shorter than that of the observed product to a sufficient extent that the detected yield can be treated as the cumulative chain yield including precursors. These two cases are denoted ind and cum, respectively, in Table I. In making this analysis, feeding during irradiation also needs to be taken into account. In some cases, although good measurements of product yields following irradiation can be made, it is impossible to interpret these as either truly independent or fully cumulative yields, and so no meaningful cross section can be extracted. In the present work this is the case for the product ^{104}Ag, since it is impossible to establish the extent of feeding from ^{104}Cd via $^{104}Ag^m$ to ^{104}Ag (and decay of ^{104}Ag) during irradiation; accordingly, this product has been excluded from the results even though large yields of it were observed.

Secondly, many of the nuclides studied have isomeric states with decay properties different from the ground state. In some cases the isomeric state decays principally via the ground state, so that the measured yield includes both states (these cases are denoted $g+m$ in Table I); in other cases the two states should be studied independently. In the present work, no case was found where both members of an isomeric doublet were detected independently, and in all cases apart from $^{92}Nb^m$ only the high spin member was detected, even though it should generally have been possible to detect the other member had it been present. It appears therefore that even in those cases where only one of the two states was measured, the yield may be treated as the total yield of that nuclide. The exception is ^{92}Nb, where the low spin isomer $^{92}Nb^m$ was detected; in this case it seems likely that the ground state ^{92}Nb may also have been populated independently, but the measurements performed were not sensitive to the presence of this state.

TABLE I. Residue cross sections (mb) measured at 106 and 148 MeV, together with the predicted contributions of the various fusion processes [complete fusion (CF) and five distinct incomplete fusion processes] modeled as described in Sec. IV. The γ-ray energies used to determine measured yields are also listed. cum denotes the cumulative chain yield including all β-decay precursors; ind denotes an independent yield.

				106 MeV								148 MeV								
		E_γ		Meas.			Modeled fusion yields					Meas.			Modeled fusion yields					
Nuclide	Half-life	(keV)	Mode	yield	Total	CF	(^{20}Ne,α)	(^{20}Ne,^{12}C)	(^{20}Ne,^{14}N)	(^{20}Ne,^{16}O)		yield	Total	CF	(^{20}Ne,α)	(^{20}Ne,^{10}B)	(^{20}Ne,^{12}C)	(^{20}Ne^{14}N)	(^{20}Ne,^{16}O)	Recoil distrib.
$^{109}In^{g+m}$	4.2 h	203.5	cum	125	162	162														*
^{108}Sn	10.3 min	396.5	cum	90	65	65														
$^{108}In^{m}$	58 min	875.5	ind	120	100	100						7	3.7	3.7						cum
$^{107}In^{g+m}$	32.4 min	205.0	cum	50	67	60	7					49	51	51						*
$^{105}Ag^{g+m}$	41.0 d	344.5	cum	147	159	145	14					98	94	75	19					*
^{104}Cd	57.7 min	709.3	cum	14	19	19	0.3					66	70	51	19					*
$^{103}Ag^{g+m}$	65.7 min	118.7	cum	31	37	19	18					150	164	140	24					*
^{101}Pd	8.47 h	296.3	cum		1.8	1.7	0.1					91	102	48	53	1.3				
$^{101}Rh^{m}$	4.34 d	306.8	ind	3.7	1.0		0.7	0.3				16	21	10	10	0.6	0.2			cum
^{100}Pd	3.63 d	539.6	cum									40	68	44	22	2.1				
^{100}Rh	20.8 h	539.6	ind	4.1	2.8	0.5	1.2	1.1				25	20	10	8	1.5	0.9			*
^{99}Pd	21.4 min	136.0	cum									4.3	9.2	6.5	1.7	1.0				
$^{99}Rh^{m}$	4.7 h	340.6	ind	7.5	9.6		0.7	8.9				22	21	5.6	9	2.2	4.2			cum
$^{97}Rh^{g}$	31.1 min	421.5	cum									5.4	14	3.1	3.8		7.4			cum
^{97}Ru	2.9 d	215.7	ind	6.6	9.7				9.7			23	33	4.3	6.2	1.1	12.5	9.4		cum
$^{96}Tc^{g+m}$	4.28 d	778.2	ind	34	9				0.3	9		23	14		0.4	0.2	1.4	4.2	8	*
$^{95}Tc^{g}$	20.0 h	765.8	cum	29	24					24		54	42		1.7	0.4	5.1	11.2	24	*
$^{94}Tc^{g}$	4.88 h	871.0	ind	7.2	8					8		28	27				3.5	2.6	21	*
$^{93}Tc^{g}$	2.75 h	1363.0	cum									7.7	10						10	*
$^{93}Mo^{m}$	6.85 h	684.7	ind	3.8								14								
$^{92}Nb^{m}$	10.2 d	934.5	ind	12								18								
$^{90}Nb^{g+m}$	14.6 h	1129.1	cum									11								
$^{89}Zr^{g+m}$	78.4 h	909.2	cum									8								
^{88}Zr	83.4 d	392.9	cum									8								
$^{87}Y^{m}$	12.7 h	381.1	cum									4								

The results obtained from this study are listed in Table I.

C. Recoil distributions

Differential recoil range distributions for a number of radioactive product residues from the reactions of ^{20}Ne with ^{93}Nb were measured at incident energies of 106 and 148 MeV using the technique reported previously.[1,11]

At each energy, the ^{20}Ne beam from the VEC was collimated to a spot diameter of 5 mm and used to irradiate a stack of foils mounted inside an electrically-suppressed Faraday cup, at a current of approximately 20 particle nA to a total fluence of approximately 300 particle μC.

In each case, the foil stack comprised a thin target followed by approximately 25 thin aluminum catchers, mounted in a close geometry. The target consisted of approximately 100 $\mu g/cm^2$ niobium evaporated onto a support of 100 $\mu g/cm^2$ Al, and was mounted with the support upstream, so that the catcher stack followed immediately after the Nb layer. The catchers used were evaporated aluminum foils, typically 100 $\mu g/cm^2$ thick; the thickness of each individual catcher foil was determined prior to use, to an uncertainty of approximately 5%, by measuring the energy lost by 5.8 MeV alpha particles from a ^{244}Cm source in traversing the foil. The targets and catchers were all mounted on thin annular holders with an internal diameter of 15 mm.

Following each irradiation, the distributions through the catcher stack of radioactive product residues recoiling from the target layer were determined by γ-ray spectrometry. Each catcher was counted against the face of one of two Ge(Li) detectors at intervals over a period of several days following irradiation; the code GAMANAL (Ref. 9) was used to find and integrate the peaks in the resulting γ-ray spectra, and decay curve analysis used to extract the relative yields of various products in the different catcher foils, as described in Sec. II B.

To obtain the recoil distribution for each nuclide, the measured yield in each catcher was divided by the measured thickness of that catcher. A correction was applied to account for the use of two different Ge(Li) detectors of different efficiency (with alternate catchers being counted on a given detector); the required correction factor for each nuclide was established from a sequence of counts in which the roles of the two detectors were interchanged.

No attempt was made to obtain absolute cross sections in this measurement, which simply determined the detailed shape of each recoil distribution, to an uncertainty of typically 10%. The absolute production cross section for each residue was instead taken from the measurements described in Sec. II B, and this value was used to normalize each corresponding recoil distribution.

The nuclides for which recoil distributions were measured are noted in Table I, together with the γ-ray lines used. It should be noted that in some cases the recoil distribution was measured only for a cumulative yield where cross sections had previously been measured for individual nuclides.

III. SUMMARY OF THE DATA

A. Particle spectra

1. Boron, carbon, nitrogen

The spectra of carbon and nitrogen ejectiles observed at 106 MeV, and of boron, carbon, and nitrogen observed at 148 MeV, are shown in Figs. 2 and 3 (no significant yield of boron was observed at the lower energy).

The energy spectra are all rather similar, consisting of a broad, symmetric peak, whose energy decreases slightly with angle and whose intensity falls off exponentially with angle. In each case the energy of the peak at the most forward angle is slightly below the energy corresponding to beam velocity for that species (treating the detected ions as ^{10}B, ^{12}C, and ^{14}N).

The differential cross section, $d\sigma/d\Omega$, for each species as a function of laboratory angle was obtained by integrating the energy spectrum measured at each angle. The results are plotted in Fig. 6, and show, as already noted, that the cross section falls off exponentially with angle.

These spectra are thus qualitatively as expected for fragments from projectile breakup, and are similar to those previously observed in association with incomplete fusion.[1,5] The fact that no evidence was found of emitted lithium or beryllium fragments (although of course ^{8}Be would not in any case be detected as such) lends weight to

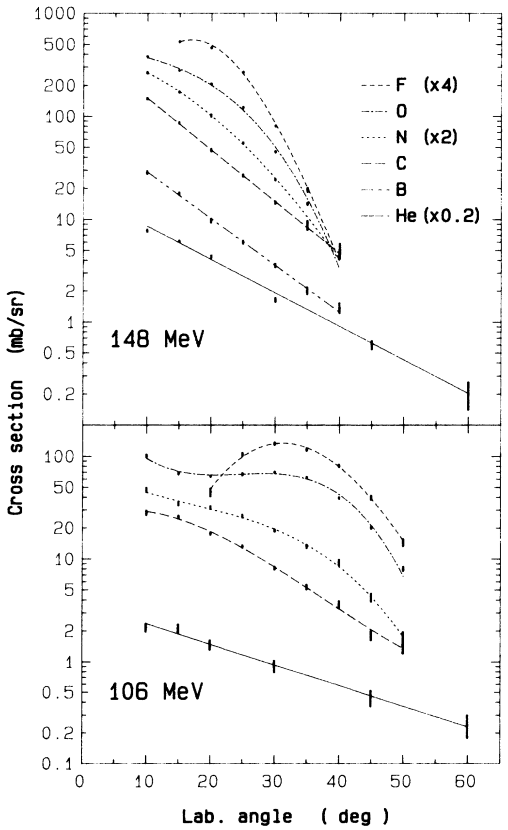

FIG. 6. Angular distributions (lab differential cross sections) of emitted projectilelike fragments, and of the nonevaporative component of the alpha particle spectra.

the suggestion that the observed fragments are associated with incomplete fusion rather than simple projectile breakup.

In previous work on $^{12}C + {}^{51}V$ reactions,[1] it was shown that spectra such as these can be fitted quite satisfactorily using the purely empirical form

$$\frac{d^2\sigma}{dE\,d\Omega}(E,\theta)=A\exp\left[-\frac{\theta}{\theta_0}\right]\mathrm{sech}\left[\frac{E-E_0-k\theta}{\omega}\right]. \quad (1)$$

The same form has been used to parametrize the spectra considered here, and the parameters E_0,k,ω,θ_0 (obtained by least-squares fitting to the data) have been used to represent these spectra for the purpose of the modeling to be discussed in Sec. IV.

2. Oxygen and fluorine

The spectra of oxygen ejectiles shown in Figs. 2 and 3 are more complex than those of the lighter ions, and apparently contain two components. As well as a broad component, similar to those observed in the spectra of boron, carbon, and nitrogen, characteristic of projectile breakup or incomplete fusion, there is also a narrower component at somewhat higher energy. Whereas the intensity of the broad component falls off exponentially with angle, the narrow component peaks at a nonzero angle, as might be expected from a grazing transfer process.

For the sake of obtaining a parametrized form of these spectra, and in an attempt to separate the two components, we have attempted to fit the measured oxygen spectra using two components, one appropriate for breakup or incomplete fusion, as used for the other spectra, and one of the form

$$\frac{d^2\sigma}{dE\,d\Omega}(E,\theta)=B\exp\left[\frac{-(\theta-\theta_t)^2}{\omega_\theta^2}\right]\times\exp\left[\frac{-(E-E_t-\kappa\theta)^2}{\omega_E^2}\right], \quad (2)$$

which we considered appropriate to describe the angular distribution for particle transfer. In practice it was found that much better results were obtained using a form asymmetric in energy for the broad incomplete fusion component, and so for the purpose of fitting the oxygen spectra a function of the form

$$A\exp\left[-\frac{\theta}{\theta_0}\right]\times\frac{1}{\exp\left[\frac{E-E_0-k\theta}{\omega_1}\right]+\exp\left[-\frac{E-E_0-k\theta}{\omega_2}\right]} \quad (3)$$

was used to represent the broad component, instead of the sech function used previously. Excellent results were obtained by fitting a superposition of (2) and (3) to the data; the curves in Figs. 2 and 3 show the two distinct components which go to make up this parametrization.

This analysis indicates that the narrow component in the oxygen spectra peaks at about 32° at 106 MeV and at about 19° at 148 MeV; these angles correspond to classical trajectories with distances of closest approach of around 13 fm, much larger than the half-density separation usually associated with fusion processes (about 8 fm). This suggests that the narrow component in these spectra corresponds to direct transfer processes occurring at much larger impact parameters than expected to contribute to incomplete fusion.

The fluorine spectra show similar features, but the broad component is much weaker; unfortunately, due to contamination of the spectra by the strong elastic scattering peak, it proved impossible to measure the fluorine spectra at the most forward angles. The narrow component of these spectra shows structure corresponding to excitation of discrete levels.

3. Protons and alphas

The spectra of protons and alpha particles measured at 148 MeV (Figs. 4 and 5) appear qualitatively consistent with particles evaporated during deexcitation of the compound nucleus. Such evaporation spectra must show symmetry about 90° in the center of mass frame; when viewed, as here, in the laboratory frame they are displaced towards forward angles. Comparison with detailed modeling based on this symmetry requirement, to be discussed in Sec. IV, reveals, however, a second component in the alpha spectra, similar to the broad component observed in the spectra of the heavier species.

4. Summary

The measured particle spectra clearly show at least three types of component: (i) particles evaporated during deexcitation of excited intermediates (protons and alphas); (ii) a broad component, centered approximately at beam velocity, whose intensity falls off exponentially with angle, attributable to projectile breakup or incomplete fusion

TABLE II. Estimated total yields of projectilelike fragments (mb). The values in parentheses indicate the yield over the range of angles actually studied. For oxygen, the yield has been decomposed into a component typical of incomplete fusion and a transferlike component; the same two components are present for fluorine but cannot be separated. The alpha-particle yield listed does not include the evaporative component.

	106 MeV		148 MeV	
Fluorine	40		70	
	(37)		(55)	
Oxygen	125 (105)	55 ICF 70 transfer	215 (150)	140 ICF 75 transfer
Nitrogen	20		56	
	(17)		(40)	
Carbon	20		66	
	(17)		(40)	
Boron				
			(9)	
Alphas	120		270	

(seen in all spectra from boron up, and also present in alpha spectra); and (iii) a narrow component peaking at a characteristic grazing angle, attributable to particle transfer processes (oxygen and fluorine spectra).

The total yield,

$$2\pi \int \sin\theta \frac{d\sigma}{d\Omega} d\theta ,$$

of each emitted species can be estimated by extrapolating the measured values of $d\sigma/d\Omega$, shown in Fig. 6, forward to 0°. Table II lists the resulting estimates for the total yields of ejectiles with $Z \geq 5$ (the values for alphas are extracted by the analysis to be discussed in Sec. IV); the figures in parentheses indicate the observed yield integrated only over the range of angles actually studied (generally down to 10°).

B. Recoil range distributions

The projected range distribution of a recoiling reaction product reflects its velocity distribution following the reaction. For a product formed by particle evaporation from a recoiling intermediate with a well-defined velocity v_0, the velocity distribution will be symmetric about v_0, with a width which depends upon the evaporation process (and, in particular, upon the number of alpha particles, as opposed to nucleons, evaporated). For the compound nucleus formed by complete fusion

$$v_0 = v_{CN} \equiv \frac{\sqrt{2mE}}{M}$$

(where m is the projectile mass, M the total mass of the system, and E the incident laboratory energy); for an intermediate formed by any other process, the recoil velocity will be less than this value.

1. Results at 106 MeV

The distributions measured at 106 MeV for the three indium isotopes and the two silver isotopes (Fig. 7) are qualitatively as expected for residues resulting from particle evaporation from the ^{113}Sb compound nucleus formed in complete fusion. Each comprises a relatively narrow, symmetric peak, centered approximately at the depth corresponding to a recoil velocity of v_{CN}. The widths of the distributions are greater for the silver isotopes than the indium isotopes, as expected if the latter arise purely from nucleon evaporation from the compound nucleus, whereas production of the former involves evaporation of an alpha particle.

In contrast, the distributions for ^{99}Rh and ^{97}Ru each show a relatively narrow but asymmetric peak centered at a much shallower depth. At this incident energy, it is energetically impossible to populate these products by evaporation following complete fusion, so that they must be formed by some type of incomplete fusion process. It is most likely that these products are principally formed by evaporation of two neutrons from the intermediates $^{101}Rh^*$ and $^{99}Ru^*$, respectively, formed by the incomplete fusion processes $^{93}Nb(^{20}Ne,^{12}C)^{101}Rh^*$ and $^{93}Nb(^{20}Ne,^{14}N)^{99}Ru^*$. This point will be discussed further in Sec. V.

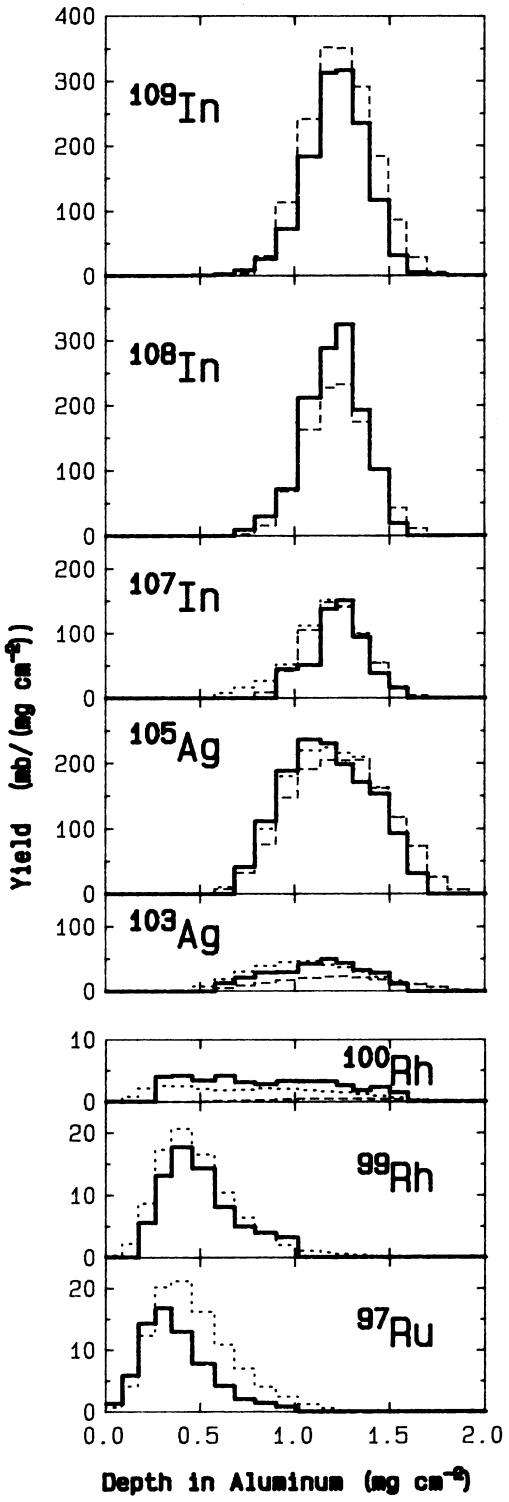

FIG. 7. Recoil distributions measured for products above mass 96 at 106 MeV (solid histograms). The dashed histograms show the results of modeling for complete fusion alone, the dotted histograms show the modeled results incorporating incomplete fusion processes also.

The product ^{100}Rh shows a much a broader recoil distribution, which presumably contains components due to both complete and incomplete fusion.

The products with $A \leq 96$ (Fig. 9) all show very shallow recoil distributions, corresponding to very little momentum transfer in the reaction; such distributions might result either from incomplete fusion of a single alpha particle with the target or from a direct transfer process.

2. *Results at 148 MeV*

The distributions measured at 148 MeV (Figs. 8 and 9) show the same general features as those at the lower energy, but the individual distributions are generally more complex and mostly appear to contain several overlapping components. Once again, at the two extremes, we have distributions qualitatively as expected from complete fusion for the heaviest observed products (^{108}In, ^{105}Ag), and very shallow distributions for the products with

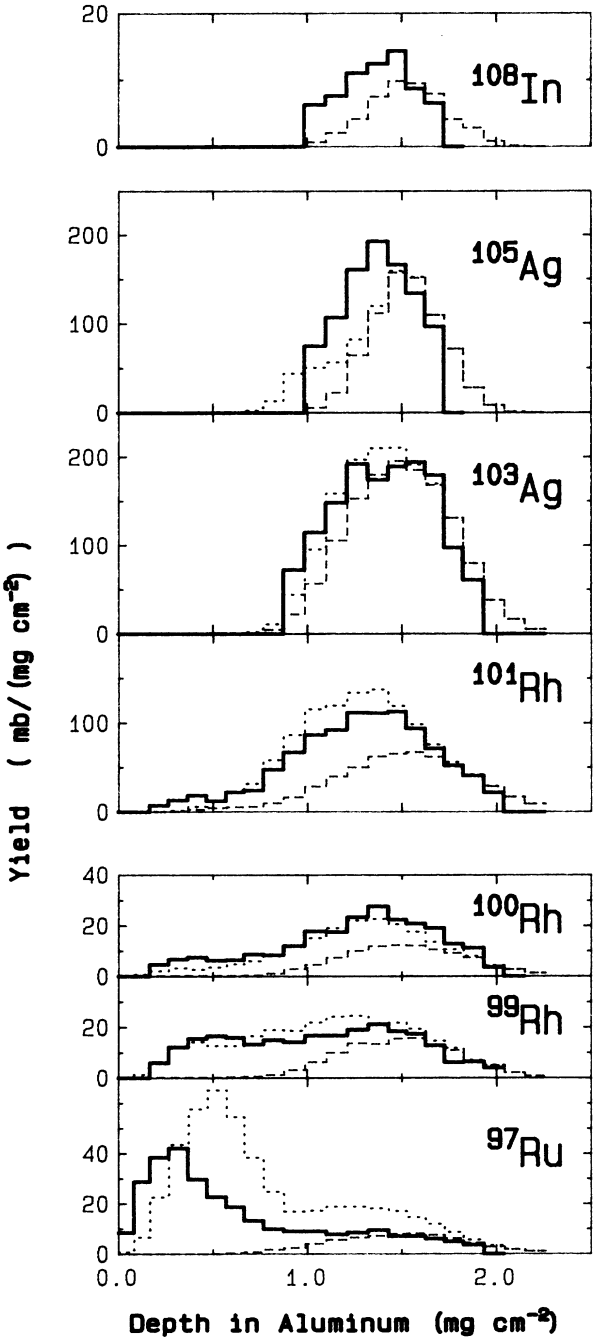

FIG. 8. As Fig. 7, at 148 MeV.

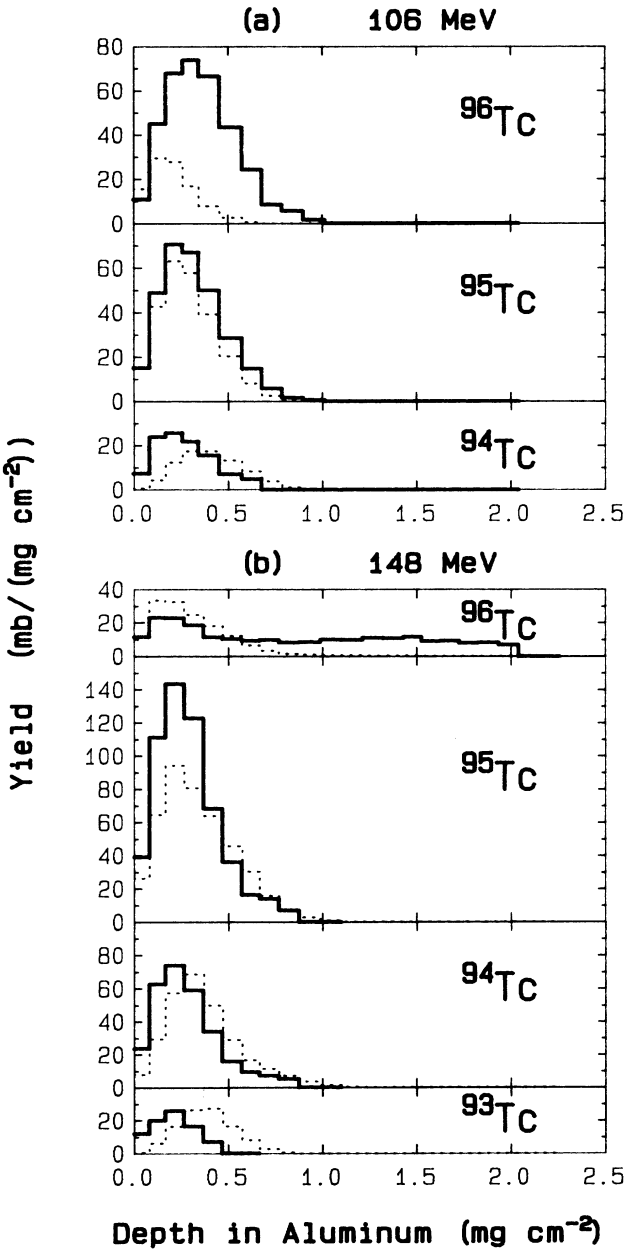

FIG. 9. As Fig. 7, for products with $93 \leq A \leq 96$ at both energies.

$A \leq 95$. In between, however, the products have broad distributions, each of which contains more than one component corresponding to distinct complete and incomplete fusion processes, but the individual components are not clearly resolved.

IV. INTERPRETATION OF THE DATA

The measured particle spectra show fragments characteristic of projectile breakup. The measured recoil distributions of the heavy residues show evidence of incomplete fuison occurring (in addition to complete fusion). It is appropriate to ask whether the two are consistent, since the observed projectilelike fragments must include the spectator fragments from any incomplete fusion processes which are present. As an extreme case, we make the hypothesis that in fact *all* of the observed projectile breakup fragments are actually associated with incomplete fusion, and investigate whether the measured recoil distributions can be quantitatively accounted for on this basis. This hypothesis was found to be substantiated in the previous study of $^{12}C + ^{51}V$.[1]

We treat both complete fusion and incomplete fusion as two stage processes in which the first stage (the "fusion stage") involves fusion of all or part of the projectile with the target nucleus to form an excited intermediate, and the second stage (the "evaporation stage") consists of deexcitation of this intermediate by particle evaporation and γ-ray emission to form the final product residue.

Whereas the compound nucleus formed in complete fusion recoils along the beam axis with a recoil velocity and excitation energy which depend simply upon the incident energy of the projectile, the intermediate formed by a particular incomplete fusion process at a given incident energy is populated with an extended distribution of recoil velocities, recoil angles, and excitation energies. The fusion stage of an incomplete fusion process can be treated as a two-body process, in which part of the projectile fuses with the target, forming the excited intermediate which recoils, while the remainder (the "spectator") continues with somewhat perturbed velocity. In a particular reaction, if the velocity and angle of emission of the spectator fragment are known, the recoil velocity and angle of the intermediate may be immediately deduced from conservation of momentum. If, furthermore, we assume that the spectator fragment is not excited, the excitation energy of the intermediate may be deduced from the difference in total kinetic energy before and after fusion and the ground state Q value for the transfer process. Thus for each incomplete fusion process, if the distribution of energies and angles of the appropriate fragment species is measured, the distribution of recoil velocities, angles, and excitation energies with which the intermediate is populated may be deduced.

If the evaporation stage of the complete or incomplete fusion process involves only statistical evaporation, the probability of a given intermediate decaying to a particular final residue depends only upon the excitation energy and angular momentum of the intermediate, and can be calculated using a statistical model code.

As described in the next section, we have used our measured projectile breakup fragment spectra to calculate the distributions of recoil velocity for the corresponding incomplete fusion intermediates, on the hypothesis that all of the observed breakup fragments are spectator fragments from incomplete fusion. We have calculated the shape of the recoil distribution for each residue formed by particle evaporation from these intermediates, as well as the shape of the recoil distribution for each residue resulting from complete fusion. The statistical model code CASCADE (Ref. 7) has been used to calculate the probabilities for forming individual residues from complete fusion and from the various incomplete fusion processes, where the excitation energy distribution of each incomplete fusion intermediate is calculated from the corresponding fragment spectra; reasonable assumptions have been made concerning the angular momenta involved. CASCADE has also been used to model the evaporation spectra of protons and alphas for comparison with the measured spectra.

The details of this modeling, most of which is similar to that previously applied to the $^{12}C + ^{51}V$ study,[1] are summarized below. In Sec. V recoil distributions modeled in this way are compared to the measured distributions, and the results discussed.

A. Fusion stage

For each incomplete fusion process, at each incident energy, we have used a Monte Carlo method to derive the distribution of excitation energies with which the intermediate is populated, from the measured spectra of the associated spectator fragment, as follows: the observed laboratory distribution of the spectator fragment was parametrized as discussed in Sec. III A, values for the velocity and angle of emission of this fragment were randomly selected from this distribution, and the corresponding excitation energy for the intermediate calculated from conservation of momentum and energy (assuming the spectator to be emitted in its ground state); this process was repeated a large number of times. The resulting distribution of excitation energies was used as the basis of the evaporation calculations described below.

A similar approach was used as the basis of the Monte Carlo modeling of the shapes of the recoil distributions for residues from incomplete fusion, described in Sec. IV C.

For both complete and incomplete fusion, it remains to specify the angular momentum with which the intermediate is populated, since this affects the subsequent evaporation process. The simplest proposed model of incomplete fusion[12] assumes that complete fusion occurs for all partial waves up to some limiting angular momentum l_{cr}, and that the various incomplete fusion processes occur in successive angular momentum bins above l_{cr}. Although the idea of exact bins is clearly an oversimplification, this basic picture appears to be supported by experimental ob-

servations, (including studies in which the angular momentum involved in incomplete fusion was deduced from measured γ-ray multiplicities[13]) and has been adopted as the basis for the modeling used here.

It is also often assumed[12] that the total cross section for all fusion processes (complete and incomplete) is equal to the hard grazing cross section, bounded by the partial wave l_{hg} for which the projectile and target just overlap to their half-density radii. Taking the values of these radii from the parametrization of Myers,[14] and using the form of the liquid drop nuclear potential suggested by Wilczynski and Siwek-Wilczynska,[15] the hard grazing cross section for ^{20}Ne on ^{93}Nb is calculated to be 1130 mb at 106 MeV and 1330 mb at 148 MeV ($l_{hg}=49$ and 63, respectively). This value should be compared with the total observed yield of projectilelike fragments (excluding the transfer component in the oxygen and fluorine spectra, but including the breakup component in the alpha spectra extracted as described in Sec. IV B) which is approximately 240 mb at 106 MeV and approximately 600 mb at 148 MeV. From a strict application of the two hypotheses that the observed fragments provide an exact measure of the incomplete fusion cross section and that the total fusion cross section (complete plus incomplete) is equal to the hard grazing value, one would deduce the cross section for complete fusion, at each energy, to be equal to the difference between the two, namely 890 mb at 106 MeV and 730 mb at 148 MeV. In fact, use of a value of 800 mb for the complete fusion cross section appears to reproduce the data quite well at both energies. This corresponds to an effective value of l_{cr} of 41 at 106 MeV and 49 at 148 MeV.

According to this picture, incomplete fusion will occur principally for incident partial waves between l_{cr} and l_{hg}, that is, for $l=41$–49 at 106 MeV and for $l=49$–63 at 148 MeV. However, the angular momentum with which the incomplete fusion intermediate is populated must always be less than the incident value, since some of the incident angular momentum must be carried off by the spectator. If the projectile were a point object, the incident angular momentum would be shared between the fusing fragment and the spectator in the ratio of their masses; since the diameter of the projectile in fact extends over a range of impact parameters and in general the spectator presumably breaks off from the *outside* of the projectile, the angular momentum imparted to the intermediate by a fusing fragment of mass m_f coming from a projectile of mass m incident with angular momentum l_{inc} will presumably in general be somewhat less than $(m_f/m)l_{inc}$. For simplicity it is probably not unrealistic to make the approximation that, for a given incident projectile energy, the angular momentum imparted to the intermediate is proportional to the mass of the fusing fragment, despite the fact that different ranges of impact parameters are probably associated with the different incomplete fusion processes, since this effect is counteracted by the geometrical effect just mentioned. In the present modeling, the various incomplete fusion processes were assumed to populate their respective intermediates with a spin equal to $2.2m_f$ at 106 MeV, and $2.6m_f$ at 148 MeV (m_f in u).

B. Evaporation stage: CASCADE calculations

The statistical model code CASCADE (Ref. 7) was used to model the process of deexcitation by successive particle evaporation, following complete or incomplete fusion, in order to predict the relative yields of individual residues and to calculate the corresponding evaporation spectra.

In general, the default parameters recommended for this mass regime were used. However, comparison with the data indicated that CASCADE calculations performed using exclusively default parameters systematically overestimated the degree of particle evaporation, and it was found to be necessary to increase the relative importance of γ-ray emission in the deexcitation process. Accordingly, the calculations reported here were performed using an $E2$ γ-ray transition strength of 100 Weisskopf units (W.u.), rather than the default value of 5 W.u. A value of this magnitude is not physically unreasonable; the effect on the calculated results is significant but not dramatic.

For complete fusion, as discussed in the preceding section, a strong absorption form for the fusion cross section was used, in which all partial waves up to some limiting value lead to complete fusion; the complete fusion cross section was taken equal to 800 mb at both incident energies.

For each incomplete fusion process, the intermediate is populated with an extended range of excitation energies. Accordingly, CASCADE calculations were performed over the whole range of possible excitation energies, and the results weighted according to the predicted excitation distribution of the intermediate, calculated, as described in the preceding section, from the distribution of the associated spectator fragment. These CASCADE calculations were performed on the basis that each intermediate is populated with a single initial spin, as discussed in the preceding section.

As well as the yields of final residues, CASCADE also calculates the center of mass energy spectrum of evaporated protons and alpha particles. In order to compare these with our measured spectra, it is necessary to transform the calculated spectra into the laboratory frame, and to postulate some angular distribution. Since the angular distribution is necessarily symmetric about 90°, we have parametrized it as

$$\frac{d\sigma}{d\Omega}=\frac{1}{4\pi}\left[a+3b\cos^2\bar{\theta}+\frac{2c}{\pi\sin\bar{\theta}}\right],$$

(where $\bar{\theta}$ is the angle measured in the center of mass frame) and determined the parameters a,b,c by fitting to the data, after transformation into the laboratory frame. The smooth curves in Fig. 4 show the spectra of evaporated protons calculated by CASCADE for complete fusion, transformed, and fitted to the data in this way. Although the calculated curves differ to some extent from the observed spectra (in particular, the calculated Coulomb barrier for proton emission appears to be a little too high), there is no indication of any strongly forward peaked component in these spectra.

The total yield of evaporated protons is proportional, in this parametrization, to the sum $a+b+c$; rather than

fixing this equal to unity (which would correspond to the yield predicted by CASCADE), the parameters in the fitting process were varied without constraint. In fact, the fitted curves shown in Fig. 4 correspond to a total evaporative yield of 2000 mb, whereas CASCADE predicts a yield of 1500 mb of protons evaporated following complete fusion. A large part of this difference is easily explained as due to the additional presence of protons evaporated following the various incomplete fusion processes; when these are modeled, a total yield of approximately 400 mb of protons evaporated following incomplete fusion is predicted at 148 MeV. Thus when both complete and incomplete fusion are considered, the CASCADE calculations reproduce the measured proton yield to within 8%.

It was found to be impossible to fit the measured alpha particle spectra, shown in Fig. 5, in this way. Instead, the spectrum calculated by CASCADE for complete fusion, transformed into the laboratory frame, has been fitted only to the spectra measured at angles from 75° backwards. The smooth curves in Fig. 5 show the resulting fit; it is apparent that an additional component is present at forward angles. When the calculated evaporation spectrum is subtracted from the measured spectrum at forward angles, this additional component (shown by the points in Fig. 5) is seen to have the characteristic projectile breakup form already observed for the heavier fragments, centered at approximately 30 MeV (alpha particles with beam velocity). This breakup component has been parametrized as described for the boron-nitrogen spectra, and used as the basis for modeling the $^{93}Nb(^{20}Ne,^{4}He)^{109}In^{*}$ incomplete fusion process; the angular distribution of this breakup component is shown in Fig. 6, and the total estimated yield of breakup alphas is listed in Table II.

The total yield of evaporative alpha particles predicted by CASCADE from complete fusion is 680 mb, whereas the fit shown in Fig. 5 corresponds to a total yield of approximately 1250 mb. Only part of this difference can be accounted for by alphas evaporated following incomplete fusion—modeling indicates that this contribution is approximately 250 mb. Thus the data indicate a yield higher by approximately 320 mb (33%) than predicted altogether for complete and incomplete fusion; this discrepancy is significantly greater than the uncertainty in the experimental normalization. While this discrepancy may well be due to the use of slightly inappropriate parameters in the CASCADE calculations, comparison with the cross sections for producing particular residues indicates that the CASCADE calculations are not significantly underestimating the degree of alpha particle evaporation. Part of the apparent difference probably arises from the fact that the analysis (and in particular the transformation from center of mass frame to the laboratory frame) was performed assuming complete fusion; for incomplete fusion the center of mass motion is reduced, so that the shift of the spectra towards forward angles is less than assumed in the analysis, leading to an overestimate of the evaporative yield at forward angles. As a corollary, the yield of breakup alphas may be somewhat underestimated, but only by approximately 10%, which does not significantly affect the discussion in Sec. V.

C. Recoil distributions

A Monte Carlo approach was used to model the shapes of the recoil distributions for individual residues resulting from complete and incomplete fusion; this has been described in detail elsewhere[1,11] and will be summarized here.

The code used simulated, for a specified sequence of particles evaporated from a given excited intermediate, the perturbing effect on the recoil velocity of the successive evaporations. At each evaporation step of each simulation, the energy of the evaporated particle was randomly chosen from a Maxwellian distribution of the form $(E-E_b)\exp(-E/T)$, where the effective barrier energy E_b for this evaporation step was taken from an appropriate CASCADE calculation and the nuclear temperature T of the emitting nucleus was derived from its excitation energy ϵ (MeV) and mass number A using the relation $T=\sqrt{8\epsilon/A}$. Likewise, the direction of emission (in three-dimensions) of the evaporated particle at each step was randomly chosen according to an appropriate angular distribution (isotropic for nucleon evaporation, somewhat anisotropic for alpha evaporation). At the end of each simulation, the final recoil velocity of the product was converted to a value of projected range, using a polynomial parametrization of the tabulation of Northcliffe and Schilling[16] for the range of that element in aluminum. Random perturbations were also introduced to simulate the effect of finite target thickness and various straggling effects. The shape of the recoil range distribution was constructed by repeating this simulation process typically 100 000 times; only simulations which were energetically allowable and which left the final residue with less than 12 MeV of excitation energy were included in constructing the final distribution.

For complete fusion, each simulation started with the compound nucleus, of known excitation energy, recoiling along the beam axis with velocity v_{CN}. In the case of incomplete fusion, for each simulation, the initial velocity, direction of recoil, and excitation energy of the intermediate were derived from values of the velocity and direction of emission of the corresponding spectator, which in turn were randomly chosen from the (parametrized) measured distribution.

The weakness of this modeling procedure is that the sequence of particle evaporations must be specified in advance, and, apart from a check on the final excitation energy of the residue, no check is made whether this is a physically probable evaporation process. In principle, this modeling should be repeated for each possible sequence of particle evaporations by which a given product may be formed; in practice it is found that the order of evaporation has no appreciable effect on the shape of the recoil distribution, and it is only necessary to establish beforehand how many alpha particles (as opposed to individual nucleons) are most probably evaporated in forming a specified product at a specified energy.

It has already been noted that several of the detected "products" are in fact produced by feeding from the original residues. For simplicity, the recoil distributions have in all cases been modeled as if the detected product were

truly the reaction residue; in general this simplification has little effect on the modeled distributions, which vary little between adjacent isobars.

V. DISCUSSION OF RESULTS

A. Comparison between data and modeled results

The dashed histograms in Figs. 7–9 show the modeled recoil distributions corresponding to complete fusion, modeled as described above; the dotted histograms show the distributions modeled on the basis of incomplete as well as complete fusion, assuming the incomplete fusion processes to be those implied by the measured projectilelike fragment spectra. The shapes of the different components contributing to each recoil distribution were modeled as described in Sec. IV C, and the magnitudes calculated as discussed in Sec. IV B.

In Table I the modeled yields of the various detected residues resulting from the different fusion processes are listed alongside the measured total yields.

Overall (with some slight exceptions which will be discussed further) when all the incomplete fusion processes are taken into account, the agreement between the modeled and measured residue yields, and between the modeled recoil distributions and the measured distributions, is rather good. In contrast, it is clear that complete fusion alone totally fails to reproduce several of the observed cross sections and recoil distributions. We may conclude therefore that incomplete fusion is indeed occurring, and that the hypothesis that essentially all the observed projectilelike fragments arise from incomplete fusion processes is not drastically wrong.

The agreement in the case of the products ^{99}Rh and ^{97}Ru at 106 MeV is particularly notable. As suggested in Sec. III B, each of these products appears to be populated principally by a single incomplete fusion process (involving emission of ^{12}C and ^{14}N, respectively); the fact that the modeling reproduces these two measured distributions so well adds considerable weight to the intepretation.

As well as the various assumptions and choices of parameters, discussed in Sec. IV, which affect the modeled distributions, some further points need to be discussed. In particular, since the mass of the detected ion could not in general be determined in the measured particle spectra, we have had to make assumptions as to which isotope(s) of the spectator is/are involved. The modeling shown in Figs. 7 and 8 assumed that all the detected boron, carbon, and nitrogen fragments were in fact ^{10}B, ^{12}C, and ^{14}N ions. Some evidence for these choices comes from the measured energy spectra—with a different choice of mass, the spectra would not correspond so well to beam velocity. In the case of boron and carbon, there is probably little doubt that this choice of masses is correct (it is considered unlikely that ^{20}Ne will fragment into ^{11}B+^{9}B or into ^{7}Be + ^{13}C), but in the case of nitorgen one might expect at least as much ^{15}N as ^{14}N to be produced, from Q-value arguments. However, it is impossible to reproduce the observed data for ^{97}Ru on the basis of ^{15}N rather than ^{14}N emission; accordingly the assumption has been made that all of the observed nitrogen may be treated as ^{14}N.

A similar ambiguity arises with regard to the possibility of ^{8}Be emission. It is known from previous studies[1,17] that ^{8}Be may be emitted as a spectator in incomplete fusion, but breaks up into two alpha particles before detection. It is possible that part of the observed yield of breakup alphas should in fact be treated as ^{8}Be (with twice the energy and half the yield). While the data are not really sufficiently sensitive to the difference between these two processes to determine whether ^{8}Be emission may be contributing at a low level, we have found that reasonable agreement with the data can be achieved without invoking any ^{8}Be emission, and the modeling shown here assumes that all of the observed alpha fragments are indeed emitted as alphas.

The modeling fails to reproduce adequately the measured recoil distributions for ^{108}In and ^{105}Ag at 148 MeV. The shift in peak position seen in these distributions is similar to that observed in previous studies of high energy alpha-induced reactions[18] and attributed to preequilibrium emission from the compound nucleus; it is possible that this is the explanation for this discrepancy.

The only other major discrepancy between modeled and measured distributions in Figs. 7 and 8 occurs for production of ^{97}Ru at 148 MeV. Here the modeling apparently overestimates the yield of this residue arising from all fusion modes except ^{93}Nb(^{20}Ne,^{14}N)^{99}Ru* by approximately a factor of 2, and somewhat underestimates the contribution corresponding to emission of nitrogen (modeling suggests that this process contributes less than the process ^{93}Nb(^{20}Ne,^{12}C)^{101}Rh*, whereas the data suggest the reverse). The factor of 2 discrepancy in absolute cross section is presumably due to an inadequacy in the level densities used for this nuclide. The underestimate in the nitrogen emission contribution is perhaps more surprising; once again, the situation is worsened if ^{15}N emission is tried in place of ^{14}N emission.

The reverse situation is encountered for the product ^{96}Tc at 148 MeV (Fig. 9), since the CASCADE calculations fail to predict the significant contribution of complete fusion observed in the recoil distribution.

Overall, it can be seen from Table I that the modeled cross sections agree with the observed yields for products heavier than mass 96 generally to within approximately 30%, with one or two poorer cases differing by up to a factor of 2. This is considered typical of the level of agreement expected from statistical model calculations; no sustained attempt has been made to improve this agreement by varying the parameters used in CASCADE.

The dotted histograms shown in Fig. 9 represent the modeled contribution of incomplete fusion processes to forming the technetium isotopes; these are dominated by the process ^{93}Nb(^{20}Ne,^{16}O)^{97}Tc*. We have noted that a second component, characteristic of direct particle transfer, is present in the observed oxygen spectra. It is quite likely that the significant difference between the modeled and observed distributions for ^{96}Tc at 106 MeV is due to a contribution from a process of particle evaporation following direct transfer. In fact, a *transfer* process ^{93}Nb(^{20}Ne,^{16}O)^{97}Tc* would be expected to populate

the ^{97}Tc intermediate with an excitation energy appropriate to evaporate one neutron at 106 MeV and two neutrons at 148 MeV, and indeed, at the two incident energies, the observed yields of ^{96}Tc and ^{95}Tc, respectively, are higher than modeled assuming simply incomplete fusion. As in our previous study,[6] we observe that the mean range of the technetium residue decreases with decreasing mass, whereas a single incomplete fusion process would lead to the opposite trend, as lighter products require higher excitation energy for the intermediate, which in turn implies larger transfer of momentum. We suggested previously[6] that such a variation could only be explained by assuming that other transfer processes, involving smaller transfer of mass, contribute to formation of the lightest products. For example, ^{94}Tc may contain a contribution due to evaporation of a neutron following the two proton transfer reaction $^{93}Nb(^{20}Ne,^{18}O)^{95}Tc^*$.

The recoil distributions measured for products with $Z<43$ are consistent with the results on mean recoil range reported previously,[6] and add little to the discussion of near-target products in that paper.

B. Implications

The generally good agreement found between our measured data, both for the residue yields and for the shapes of the recoil distributions, and the modeled predictions, suggests that the interpretation of these reactions in terms of complete and incomplete fusion processes, and the assumption that essentially all of the yields of projectilelike fragments, listed in Table II, arise from incomplete fusion, are basically correct. Further, the assumption made in Sec. IV that the total cross section for all fusion processes (complete and incomplete) is approximately equal to the hard grazing value also appears to be validated.

This assumption is also one of the axioms of the sum rule model for incomplete fusion suggested by Wilczynski *et al.*,[19] and it is interesting to consider to what extent our results for the total cross sections of the individual fusion processes can be modeled within that framework. Although an extensive comparison has not been performed, it appears that the relative cross sections of the different fusion modes observed by us cannot be predicted from Q-value arguments, as used in Ref. 19. In particular, such Q-value arguments invariably predict a much larger cross section for the incomplete fusion process $^{93}Nb(^{20}Ne,^{15}N)^{98}Ru^*$ than for the process $^{93}Nb(^{20}Ne,^{14}N)^{99}Ru^*$, whereas our data suggest that the latter is the more important process.

While it appears that the basic picture of various incomplete fusion processes occurring in localized regions of l space appears to be generally accepted, the detailed mechanism responsible for selecting the incomplete fusion mode is probably quite complex and cannot in general be accounted for simply on the basis of Q-value arguments.

VI. CONCLUSIONS

The inclusive particle spectra of emitted boron, carbon, nitrogen, and oxygen which we have measured from reactions of 106 and 148 MeV ^{20}Ne and ^{93}Nb show components characteristic of projectile breakup; a similar component is found in the alpha particle spectra after the evaporative component is subtracted.

The differential recoil range distributions measured for a number of reaction residues show components characteristic of both complete and incomplete fusion processes. It is possible to account rather well both for the absolute yields of all the detected residues heavier than mass 96 and for the detailed shapes of the measured recoil distributions in terms of a superposition of complete and incomplete fusion processes, where the total cross section for all fusion processes was taken equal to the hard grazing value and the individual incomplete fusion contributions were determined from the measured particle spectra on the assumption that essentially all of the observed projectilelike fragments are spectator fragments accompanying incomplete fusion. The absolute yields of evaporated protons are also well accounted for on this basis; although the yield of evaporated alphas appears to be underestimated by the modeling, this is probably at least partly due to inadequacies in the analysis of the data. The complete fusion cross section appears to be approximately 800 mb at both energies studied.

The data suggest that the nitrogen fragments detected are principally ^{14}N rather than ^{15}N. This is at variance with predictions based on the sum rule model of incomplete fusion,[19] although the overall approach to the modeling taken here is quite similar to the concepts underlying that model.

There is some evidence that direct transfer processes are primarily responsible for forming near-target products; it was outside the scope of this study to identify these.

ACKNOWLEDGMENTS

The authors are grateful for helpful discussions with Prof. E. Gadioli, Dr. T. W. Conlon, and Dr. P. E. Hodgson during the course of this work. The assistance of Mr. S. Sugden in measuring the particle spectra, and of Dr. P. M. Read in preparing and analyzing targets was much appreciated. As usual we acknowledge our indebtedness to Mrs. M. Miller, who produced all the target and catcher foils used. J. J. H. was supported in this work by the Natural Sciences and Engineering Research Council of Canada and by an Exchange Grant of the Royal Society. The work described in this paper was undertaken as part of the Underlying Research Programme of the United Kingdom Atomic Energy Authority.

[1]D. J. Parker, J. Asher, T. W. Conlon, and I. Naqib, Phys. Rev. C **30**, 143 (1984).
[2]R. Kaufman and R. Wolfgang, Phys. Rev. **121**, 192 (1961).
[3]Reviewed by J. M. Alexander, in *Nuclear Chemistry,* edited by L. Yaffe (Academic, New York, 1968), Chap. 4. The paper of P. M. Strudler, I. L. Preiss, and R. Wolfgang, Phys. Rev. **154**, 1126 (1967), is of particular relevance to the present study.
[4]T. Inamura, M. Ishihara, T. Fukuda, T. Shimado, and H. Hiruta, Phys. Lett. **68B**, 51 (1977).
[5]See reviews by C. Gerschel, Nucl. Phys. **A387**, 297c (1982), and R. H. Siemssen, Nucl. Phys. **A400**, 245c (1983).
[6]J. J. Hogan, J. Asher, and D. J. Parker, Phys. Rev. C **31**, 477 (1985).
[7]F. Pühlhofer, Nucl. Phys. **A280**, 267 (1977).
[8]U. Littmark and J. F. Ziegler, *The Stopping and Ranges of Ions in Matter* (Pergamon, New York, 1977), Vol. 6.
[9]J. A. B. Goodall, United Kingdom Atomic Energy Authority Report AERE-M 3185, 1982.
[10]U. Reus, W. Westmeier, and I. Warnecke, At. Data Nucl. Data Tables **29**, 1 (1983).
[11]D. J. Parker, D.Phil. thesis, University of Oxford, United Kingdom Atomic Energy Authority Report AERE R-11464, 1984.
[12]K. Siwek-Wilczynska, E. H. du Marchie van Voorthuysen, J. van Popta, R. H. Siemssen, and J. Wilczynski, Nucl. Phys. **A330**, 150 (1979).
[13]T. Inamura, A. C. Kahler, D. R. Zolnowski, U. Garg, T. T. Sugihara, and M. Wakai, Phys. Rev. C **32**, 1539 (1985).
[14]W. D. Myers, Nucl. Phys. **A204**, 465 (1973).
[15]J. Wilczynski and K. Siwek-Wilczynska, Phys. Lett. **55B**, 270 (1975).
[16]L. C. Northcliffe and R. F. Schilling, Nucl. Data Tables **A7**, 233 (1970).
[17]A. N. Bice, A. C. Shotter, and J. Cerny, Nucl. Phys. **A390**, 161 (1982).
[18]E. Gadioli, E. Gadioli Erba, D. J. Parker, and J. Asher, Phys. Rev. C **32**, 1214 (1985).
[19]J. Wilczynski, K. Siwek-Wilczynska, J. van Driel, S. Gonggrijp, D. C. J. M. Hageman, R. V. F. Janssens, J. Lukasiak, and R. H. Siemssen, Phys. Rev. Lett. **45**, 606 (1980).